Excess electronic states in fluid helium

D. F. Coker[a] and B. J. Berne
Department of Chemistry, Columbia University, New York, New York 10027

(Received 4 February 1988; accepted 13 April 1988)

We study the nature of the excess electronic states in fluid helium by calculating the excess electron energies and wave functions for a set of configurations of solvent atoms taken from path integral Monte Carlo calculations on the solvated electron system. The eigenvalues and eigenfunctions for the different configurations of the solvent are used to calculate the inhomogeneously broadened density of states and absorption line shape of the excess electron over a range of fluid densities. The predictions of a simple theory of the excess electronic states in fluid helium due to Springett *et al.* [B. E. Springett, M. H. Cohen, and J. Jortner, Phys. Rev. **159**, 183 (1967)] are found to agree quite well with our computer simulation results. This simple theory, however, predicts an inhomogeneously broadened elecronic absorption linewidth which is much narrower than that obtained from simulation. It is found that the RISM-polaron theory of Nichols and Chandler [A. L. Nichols III and D. Chandler, J. Chem. Phys. **87**, 6671 (1987)] gives an absorption line shape which is in better agreement with our simulations. We observe a transition from lower energy states in which the electron is bound to density fluctuations in the fluid to the situation where the excess electron scatters through the fluid in continuum states at higher energies.

I. INTRODUCTION

The equilibrium behavior of excess electrons in simple fluids has been the subject of several recent theoretical studies[2–5] in which the quantum nature of the electron is treated using discrete path integral methods. In this paper we present the results of some calculations which go beyond these equilibrium treatments and explore the nature of the excited states of excess electrons in simple fluids. One of the aims of this paper is to demonstrate that at high densities a very simple theory of solvated electrons due to Springett *et al.*[1] can give quite reasonable predications concerning the nature of some of the excited excess electronic states.

The system we shall consider in detail here is an excess electron in helium. At fluid densities, and over a wide range of temperatures, the electron becomes localized in cavity-like density fluctuations in this system. In this study we have made the assumption that the fluid structure is not perturbed from that of the equilibrium solvated electron system upon electronic excitation. Thus, we use a series of solvent configurations obtained from path integral Monte Carlo calculations on the electron–solvent system to provide a sample of the different sorts of potential field which the electron experiences in the fluid. This Born–Oppenheimer-like approximation has been used recently to calculate the inhomogeneously broadened excess electronic absorption line shape in various polar fluids such as water[6,7] and ammonia.[8] In these polar systems the electron also becomes localized in small "bubbles" in the solvent. The main interest in these studies on polar fluids has been to try to understand the phenomena which give rise to the band shape of the experimental solvated electron absorption spectrum. These studies are complicated by the fact that the pseudopotentials describing the electron–solvent interaction in these polar systems are complex and not well understood. As such these studies have not yet resolved, e.g., what processes give rise to the high energy tail observed in the experimental absorption spectra for these systems.

The helium system considered here is much simpler than the polar solvents discussed above, thus a more detailed understanding of the behavior of the excess electronic states in this simple fluid can be obtained from our studies. In Sec. II we describe the computational techniques used to obtain the energies and wave functions of the excess electron in the "frozen" solvent configurations. In Sec. III we outline the simple theory of the excess electronic states in helium due to Springett *et al.* In Sec. IV we present the results of our calculations and compare them with the predictions of this simple theory. Finally, in Sec. V we discuss the implications of these studies and compare the excited state behavior of excess electrons in helium with the behavior observed in polar solvents.

II. METHODS

The method we use to calculate the energies and wave functions of the excess electron in a frozen fluid configuration is based on the split operator technique for solving the Schrödinger equation which was presented by Feit, Fleck, and Steiger.[9] Their procedure for calculating the eigenvalue spectrum involves following the evolution of a mixed quantum state in real time using the split operator approach, then employing a "spectral method" to analyze the trajectory. They define a time correlation function of the evolving mixed state solution and show that by Fourier analyzing this oscillatory function, the eigenvalues, and mixing coefficients of the eigenstates contained in the initial wave function can be extracted. The eigenfunctions can also be obtained from the time evolution of the mixed state solution once the eigenvalues have been determined.

The main problem with this approach is that the resolution of the eigenvalues obtained by Fourier transforming the finite sequence of time correlation function measurements is $2\pi/T$ where T is the total time for which the solution is

[a] Permanent address: Department of Chemistry, Boston University, 590 Commonwealth Ave., Boston, Massachusetts 02215.

 0021-9606/88/162128-10$02.10

propagated. Thus to obtain reasonably fine resolution for the energy spectrum, a long trajectory is required. This problem can be overcome by following the solution in imaginary time $\tau = it$.[10] Now, instead of being a sum of oscillatory functions, the imaginary time solution is a sum of exponentially growing or decaying terms

$$\psi(\mathbf{r},\tau) = \sum_n a_n \phi_n(\mathbf{r}) \exp[-E_n \tau/\hbar], \tag{2.1}$$

where E_n are the eigenvalues, $\phi_n(\mathbf{r})$ are the eigenfunctions, and a_n are the mixing coefficients. As $\tau \to \infty$ the spatial dependence of ψ will be dominated by $\phi_0(\mathbf{r})$, the lowest energy eigenfunction with nonzero amplitude in the propagating wave function. All the higher energy eigenstates will have exponentially smaller amplitudes compared to the lowest energy state as τ becomes large. Under these conditions the amplitude of the wave function will exhibit a single exponential growth or decay at a rate determined by the lowest eigenvalue E_0. At the end of each incremental propagation we calculate the normalization constant

$$\mathcal{N} = \left[\int |\psi|^2 d\mathbf{r}\right]^{1/2} \tag{2.2}$$

and renormalize the solution. If the wave function was normalized to unity at the beginning of each propagation step then the new normalization constant after a time step $\Delta\tau$ can be used to estimate the lowest eigenvalue

$$E_0 = -\frac{\ln \mathcal{N}}{\Delta\tau}. \tag{2.3}$$

This result is true only at long times when the solution becomes dominated by the lowest energy state. When the eigenvalue estimate becomes constant within some tolerance from one time step to the next, the solution is converged.

Once the lowest energy state is determined, the next highest state can be obtained by propagating a new solution, but now "filtering out" the previously determined lowest energy state. This is achieved by forcing the propagating solution to be orthogonal to the lower state at the end of each time step.[10] In general, if we have a set of previously determined orthonormal eigenstates $\{\phi_n(\mathbf{r})\}$ and a normalized wave function $\psi(\mathbf{r})$, we can construct a linear combination ψ', of these functions which is orthogonal to the eigenstates $\{\phi_n(\mathbf{r})\}$ and normalized by using Schmidt orthogonalization

$$\psi' = \frac{[\psi - \Sigma_n S_n \phi_n]}{\sqrt{1 - \Sigma_n |S_n|^2}}. \tag{2.4}$$

Here $S_n = \int \psi^* \phi_n d\mathbf{r}$ are the overlaps between the current solution and the previously determined eigenfunctions. All the lower energy states are thus removed from the propagating solution and the relative amplitudes of the higher energy states will decay exponentially giving a specific excited state solution.

One advantage of the procedure outlined above over the real time spectral analysis method of Feit *et al.*[9] is that the imaginary time approach can be applied selectively yielding only those states of interest. The spectral method gives all the states within a large energy interval, the size of which is determined by the reciprocal of the time step. In systems where the eigenvalues of interest are fairly well spaced, the excited state contributions will damp out very rapidly thus accurate energies and eigenfunctions can be determined using relatively short runs. As mentioned earlier, the uncertainty in the spectral analysis of the real time results falls like $1/T$. With the imaginary time approach, the major component of the error comes from the residual contributions of the higher energy states which damp out exponentially. Consequently, when only a few quantum states which are well separated in energy are required with high accuracy the imaginary time procedure will be considerably more efficient than the real time spectral analysis approach. When the band structure in a continuum of states is of interest the real time spectral analysis technique may be more useful. A variational procedure recently presented by Vanhimbeeck *et al.*[11] may also be useful in treating very closely spaced states. When the density of states involves both bound and continuum states a technique combining the imaginary time procedure to get the bound states followed by real time propagation of a mixed state which is held orthogonal to these bound states may be a useful way to proceed.

The method outlined above requires a procedure for propagating a solution of the Schrödinger equation in time. If we are interested in imaginary time propagation of a many-body wave function, the diffusion or quantum Monte Carlo methods[12–16] could in principle be applied. Excited states of systems containing two and three quantum particles have been studied using this technique together with an orthogonalization procedure similar to that discussed above.[17] If we are interested in the wave function of a single quantum particle moving in three dimensions, the split operator fast Fourier tranform (FFT) method[9] provides a very efficient technique for propagating the solution. We assume that over a small time step $\Delta\tau = i\Delta t$ the propagator can be split into kinetic and potential parts which operate independently. Thus, at a time $\tau_0 + \Delta\tau$ we write the wave function as

$$\psi(\mathbf{r},\tau_0 + \Delta\tau) \sim \exp\left[-\frac{\Delta\tau}{\hbar} V(\mathbf{r})\right] \exp\left[\frac{-\hbar\Delta\tau}{2m} \nabla^2\right] \psi(\mathbf{r},\tau_0). \tag{2.5}$$

This result is accurate to order $(\Delta\tau)^2$.

To proceed, we consider evaluating the one particle wave function on a rectangular grid with N points on a side in a box with side lengths L_x, L_y, L_z. The split operator method involves performing the kinetic part of the propagation in momentum space and the potential propagation in position space. Since we have the wave function at a discrete set of points in position space, the momentum space wave function can be obtained by a discrete Fourier transform. The two wave functions are thus related as follows:

$$\psi(\mathbf{r},\tau) = \sum_{l,m,n=-N/2+1}^{N/2} \Psi(\mathbf{p},\tau) \times \exp[2\pi i(lx/L_x + my/L_y + nz/L_z)], \tag{2.6}$$

where $\Psi(\mathbf{p},\tau)$ is the wave function in momentum space and the discrete momentum vectors have components $\mathbf{p} = (2\pi l/L_x, 2\pi m/L_y, 2\pi n/L_z)$. The split operator tech-

nique involves performing the potential and kinetic parts of an incremental propagation step separately in the position and momentum spaces, respectively. When the kinetic part of the propagator is applied to the wave function in momentum space we find

$$\Psi(\mathbf{p},\tau_0+\Delta\tau)=\Psi(\mathbf{p},\tau)\exp\left[-\frac{\hbar\Delta\tau}{2m}\mathbf{p}^2\right]. \tag{2.7}$$

In a similar fashion, when the potential part of the propagator is applied to the wave function in position space we obtain

$$\psi(\mathbf{r},\tau_0+\Delta\tau)=\psi(\mathbf{r},\tau)\exp\left[-\Delta\tau V(\mathbf{r})/\hbar\right]. \tag{2.8}$$

The algorithm which we use in these calculations can thus be summarized as follows:

(1) The normalized position space wave function at time τ_0, $\Psi(\mathbf{r},\tau_0)$, is Fourier transformed to give a momentum space wave function, $\Psi(\mathbf{p},\tau_0)$, according to Eq. (2.6).

(2) Equation (2.7) is used to perform the kinetic part of the propagation on $\Psi(\mathbf{p},\tau_0)$.

(3) The partially propagated momentum space wave function is then backtransformed and propagated in position space according to Eq. (2.8) completing the incremental propagation of the solution.

(4) Next we calculate the new normalization constant and determine the eigenvalue estimate according to Eqs. (2.2) and (2.3), then renormalize the wave function.

(5) If eigenfunctions have been previously determined we evaluate their overlaps with the new wave function and use Eq. (2.4) to maintain the orthogonality of the current solution to the lower energy states.

(6) We repeat the above steps many times until the eigenvalue becomes constant to within some tolerence.

Details of the path integral calculations which were performed to obtain a set of configurations of the equilibrium solvated electron system can be found in the work of Coker *et al.*[5] We conducted systematic studies of the time step size and coarseness of our spatial grid. The time step used was $\Delta\tau = 0.5$ a.u. Grids with 8, 16, and 32 points on the side of our periodic simulation box were tested and we found that the results of 16 and 32 points agreed to better than four significant figures. To determine the importance of long range corrections to the electronic eigenvalues, we reduced the size of the FFT box relative to the simulation box by $\sim 25\%$ and observed a systematic increase of a few percent in all the electronic eigenvalues. The differences in eigenenergies used in the spectrum calculation, however, did not change appreciably. Thus, any long range corrections seem about the same for all the eigenvalues of interest and they cancel when the excitation energies are calculated.

Except for the details, the imaginary time procedure outlined in this section was introduced by Rossky and his coworkers[6,10] and has been used by them and Wallqvist *et al.*[7] in studies of the hydrated electron. Sprik and Klein[8] have performed similar calculations on electrons in ammonia using an optimized Gaussian basis set technique which may be more efficient for studying localized states than the plane wave basis employed here. One might expect that the plane wave basis will be more useful for studying extended quasifree states. Recently, Selloni *el al.*[18] have used the plane wave basis to obtain solutions of the time dependent Schrödinger equation for an electron moving in a molten salt. This adiabatic dynamics involves propagating the motion of the solvent classically thus providing a time varying potential field for the quantum dynamics.

III. THEORETICAL MODEL

About 20 years ago, Springett *et al.*[1] developed a simple theoretical model for predicting how the equilibrium radius of the electron bubble in fluid helium should vary with pressure. Their model gave results which agreed well with experimental measurements of the bubble radii. We have used this theory to study the excited states of an excess electron in helium. In this section we present a brief description of the so-called Wigner–Seitz model[1] of the excess electron in a fluid.

Inside the bubble the electron moves through a region devoid of fluid atoms and outside, we assume that the electron scatters through a lattice of solvent particles. Figure 1 shows schematically the situation envisioned here. Following Springett *et al.* we first estimate the electronic energy barrier to penetration of the undisturbed fluid of scatterers. In the undisturbed fluid, beyond the region of the bubble, the delocalized electronic wave function $u(\mathbf{r})$ satisfies

$$\left[\frac{-\hbar^2}{2m}\nabla^2+V(\mathbf{r})\right]u(\mathbf{r})=V^0u(\mathbf{r}). \tag{3.1}$$

In the equivalent sphere of radius $r_s=(4/3\pi\rho)^{-1/3}$ centered on each solvent atom, we assume that the electron experiences a spherical potential

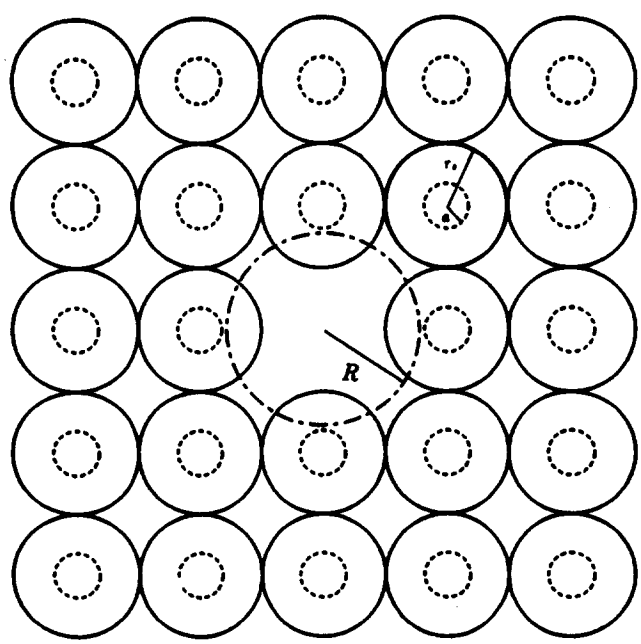

FIG. 1. Schematic diagram of the Wigner–Seitz model of the excess electron bubble and the surrounding lattice of scatterers representing the fluid.

$$V(r) = \infty, \quad r \leqslant a,$$
$$V(r) = 0, \quad 4 > a. \tag{3.2}$$

where a is the scattering length of the electron–solvent interaction and for helium $a = 1.13$ a.u.[1]

The lowest energy radial electronic wave function in the equivalent sphere is

$$u(r) = [M \sin(K_0 r) + N \cos(K_0 r)]/r, \tag{3.3}$$

where the constants M, N, and K_0 are fixed by normalization and the boundary conditions

$$u(a) = \frac{du}{dr}(r_s) = 0 \tag{3.4}$$

giving $u(r) \sim \sin[K_0(r-a)]/r$ and the eigenvalue, $V^0 = \hbar^2 K_0^2/2m$, is an estimate of the energy required to force the electron to penetrate into the fluid at this density. These undisturbed fluid results are now used to treat the bubble problem.

If the region from which the solvent atoms are excluded is of radius R we write the localized electronic wave function as follows:

$$\psi = f(\mathbf{r}), \quad r < R,$$
$$\psi = f(\mathbf{r})u(\mathbf{r}), \quad r > R, \tag{3.5}$$

and the Schrödinger equation becomes

$$\left[\frac{-\hbar^2}{2m}\nabla^2\right] f(\mathbf{r}) = E f(\mathbf{r}), \quad r < R,$$
$$\left[\frac{-\hbar^2}{2m}\nabla^2 + V\right] f(\mathbf{r})u(\mathbf{r}) = E f(\mathbf{r})u(\mathbf{r}), \quad r > R. \tag{3.6}$$

Equation (3.6) for $r > R$ simplifies by using Eq. (3.1) and assuming that $f(\mathbf{r})$ varies slowly over the Wigner–Seitz cell[1] giving

$$\left[\frac{-\hbar^2}{2m}\nabla^2 + V^0\right] f(\mathbf{r}) = E f(\mathbf{r}), \quad r > R. \tag{3.7}$$

The general radial solutions are

$$f_l(r) = j_l(q_l r), \quad r < R,$$
$$f_l(r) = A_l k_l(\kappa_l r), \quad r > R, \tag{3.8}$$

where $q_l = (2mE_l/\hbar^2)^{1/2}$ and $\kappa_l = (2m[V^0 - E_l]/\hbar^2)^{1/2}$.

The electronic energies E_l are determined by averaged boundary conditions at the edge of the bubble. An appropriate average[1] must be performed since the boundary of the bubble can cut through the Wigner–Seitz cells of the surrounding atoms anywhere the equal probability. The average boundary condition which determines the localized excess electronic energy levels is

$$\left(\frac{d \ln j_l(q_l r)}{dr}\right)_R = \left(\frac{d \ln k_l(\kappa_l r)}{dr}\right)_R. \tag{3.9}$$

It is important to note that this simple theory gives only information about states in which the excess electron is bound to the solvent cavity and V^0 is identified as the dissociation energy of the potential well provided by the cavity. Above this energy the electron will scatter through the fluid in a continuum state.

We will consider the situation at sufficiently low temperature and high density so that it can be assumed that the equilibrium size of the cavity is determined by a balance between the ground state electronic energy $E_0(R)$ and the pressure–volume and the surface work $W(R)$ required to form a bubble of radius R. Scaled particle theory[19] gives the following expression for $W(R)$ for a hard sphere fluid:

$$W(R) = C_0 + C_1 R + C_2 R^2 + C_3 R^3. \tag{3.10}$$

The constants C_n are simple functions of the hard sphere diameter, the fluid density, and the temperature.[19] In order to use the hard sphere fluid result for $W(R)$ given in Eq (3.10) to approximate the behavior of our Lennard-Jones fluid we must scale the density appropriately so that the structure of the two fluids are comparable.[5,20] Figure 2 shows the minima in the total bubble energy $E_b(R) = E_0(R) + W(R)$ for various Lennard-Jones fluid densities at $T = 309$ K and the positions of the minima give the equilibrium bubble radii R_e at these densities. Finally, we use the values of R_e together with Eqs. (3.8) and (3.9) to determine the excited state energies and wave functions for an electron bubble with the equilibrium radius. To calculate the inhomogenously broadened line shapes we used $\exp[-\beta E_b(R)]$ as the distribution function for finding an electron in a bubble of radius R in the fluid.

IV. RESULTS AND DISCUSSION

In order to compare the electron density obtained from our computer simulations with that predicted by the Wigner–Seitz model, in Fig. 3 we display the radial projection of the square of the ground state electronic wave function averaged over many solvent configurations. The Wigner–Seitz result for the averaged ground state wave function for the equilibrium bubble radius is also displayed.

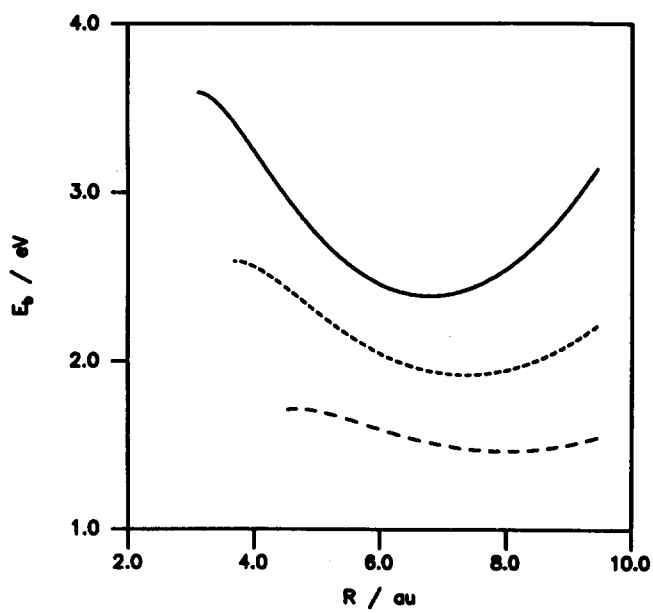

FIG. 2. Total bubble energy as a function of bubble radius. The total bubble energy is composed of the pressure–volume and surface work done against the surrounding fluid and the ground state electronic energy. Three different fluid densities are displayed $\rho^* = 0.9$ (solid), $\rho^* = 0.7$ (short dashes), and $\rho^* = 0.5$ (long dashes).

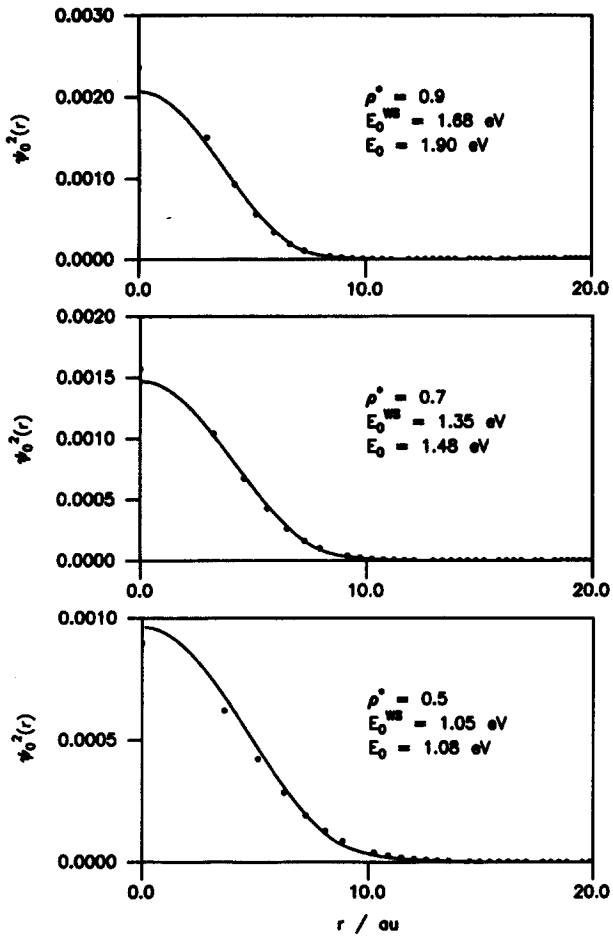

FIG. 3. Comparison of the average ground state radial electron density obtained from simulations (points) with the results predicted by the Wigner–Seitz model (curves) at various densities.

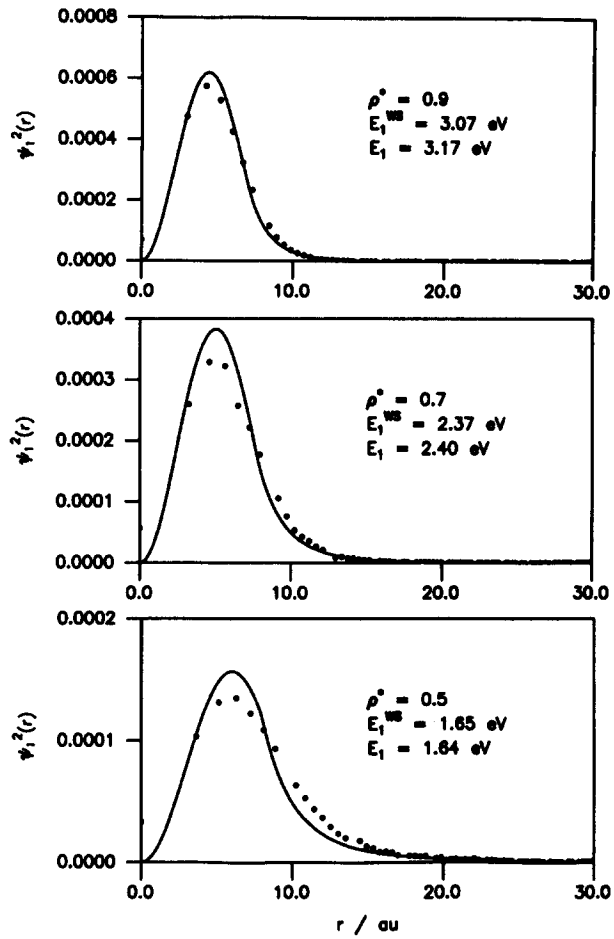

FIG. 4. Comparison of the average first excited state radial electron density obtained from simulations (points) with the results predicted by the Wigner–Seitz model (curves) at various densities.

These projections are consistently normalized so that the integral of the density in three dimensions is unity. For the computer simulation results, the radial projection was calculated using the center of mass of the path integral "beads" in each configuration as the origin. Similar results are presented for the first excited state in Fig. 4. The agreement between the simulation and theory for both the ground and first excited state for all densities is very satisfactory considering the simplicity of the Wigner–Seitz theory. Indeed, some of the differences observed, particularly for the excited state at lower densities, may result from the poor definition of the origin as the center of mass of the path integral isomorphic chain polymer.

In all the low energy electronic states considered so far, the electron is bound in the potential well provided by the cavity in the fluid. When the electronic energy exceeds the dissociation energy of this potential the electron will be in a "continuum" state and thus able to scatter through the fluid. In a macroscopic system there will be many other cavities which may act as deeper potential wells and trap the electron at these sites. Because our simulation results are obtained by averaging over an equilibrium distribution of density fluctuations for a single isolated cavity, we cannot see this "electron hopping" conduction process in our calculations.

However, there is evidence in our simulation results of a transition of the excess electron from bound to continuum states. In Fig. 5 we present the averaged radial projections of the electron density in the lowest five states obtained from our simulation studies at $\rho^* = 0.9$ and $\rho^* = 0.5$. Generally it is found that, after some short range behavior, the electron density in the lowest energy states decays to zero very rapidly as we move radially outwards from the center of the bubble. However, above a certain energy the radial density exhibits qualitatively different behavior. In these higher energy states the electron density no longer decays to zero, rather, we find that the density levels off to an appreciable nonzero value at large distances from the center of the bubble. This characteristic long tail signals the onset of continuum state behavior. Further, we see that at the lower density the onset of continuum state character occurs at smaller excitations indicating that, on average, the potential well produced by the bubble in the lower density fluid can support fewer bound states than at higher densities.

In Fig. 6 we display the density of excess electronic states obtained from our simulations. The density of states is resolved into different bands according to the order of the energy. Bands corresponding to states which have average electron density which decays to zero at large distances (i.e.,

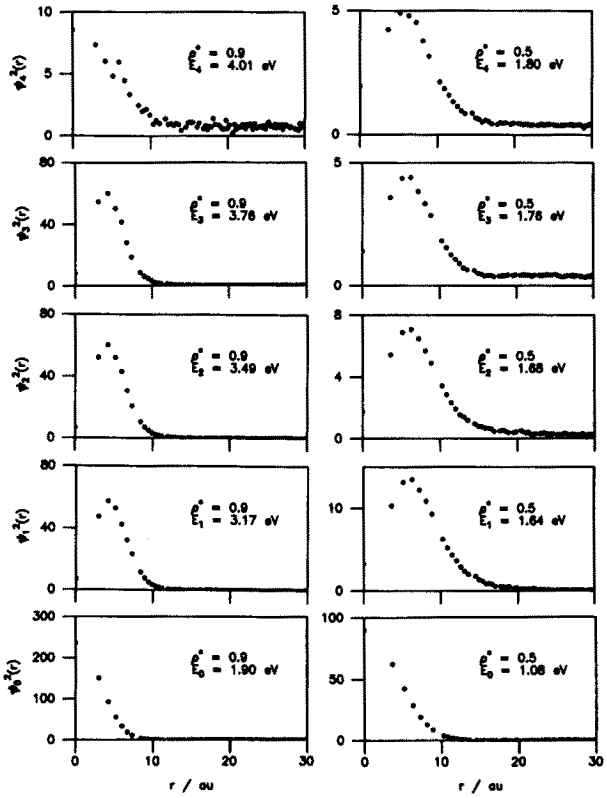

FIG. 5. Radial electron densities for different energy states obtained from simulations. Left column is for $\rho^* = 0.9$ and right column is for $\rho^* = 0.5$. The appearance of the nonzero tail at large r indicates the onset of continuum state behavior.

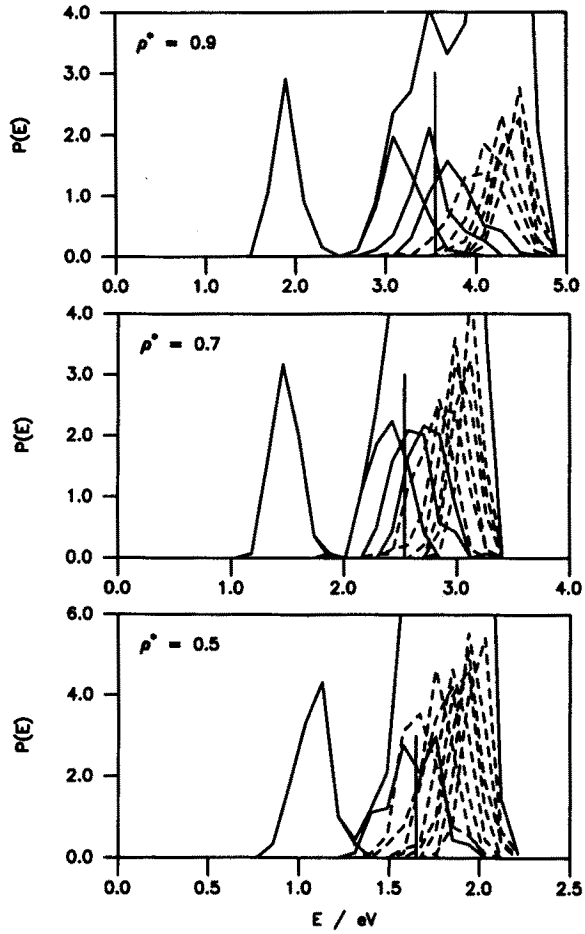

FIG. 6. Density of excess electronic states in helium. The envelope curve is the total density of states and the component break up is based on the energy. Solid lines are the bound state contributions and dashed lines are continuum state contributions. Note the change in energy scale for the different fluid densities.

bound states) are displayed with solid lines while the bands associated with the continuum states which exhibit a long range tail in the average electron density are presented as dashed lines. The barrier to electron penetration in the fluid V^0 obtained from the Wigner–Seitz model gives an estimate of the dissociation energy of the potential well provided by the solvent cavity, i.e., it approximates the electronic energy at the bottom of the "conduction band" of the fluid. The values obtained from the theory at the various densities $\rho^* = 0.9, 0.7$, and 0.5 are, respectively, $V^0 = 3.55, 2.54$, and 1.65 eV and these results are also displayed in Fig. 6. From this figure we see that these theoretical dissociation energies agree quite well with the onset of the continuum bands in the density of states.

In Fig. 7 we compare the calculated density of states with the predicted by the Wigner–Seitz model according to the following expression:

$$\rho(E) = \int dR \exp[-\beta E_b(R)] \sum_l \times \delta[E - E_l(R)] / \int dR \exp[-\beta E_b(R)]. \tag{4.1}$$

Only the bound state bands obtained from our simulations are shown in this figure. The first excited state band predicted by the Wigner–Seitz model is actually threefold degenerate so we have reduced the amplitude by a factor of 3 to enable comparison with the shape of the component bands in the simulation results. The scaled particle theory gives a reasonable description of the distribution of cavity sizes in the fluid since the shape of the ground state band agrees quite closely with the results of our calculations. In the version of the Wigner–Seitz model employed here we can say nothing about the density of states above the dissociation threshold so the theoretical densities of states are cut off above this point. From the figure we see that the theory predicts dissociation in the first excited state band at all fluid densities considered. As the density is decreased, the dissociation energy moves down through the first excited state band. Similar behavior is observed in our simulation results as the number of bound states observed decreases at lower densities. The Wigner–Seitz model predicts only a single excited state band and its shape agrees reasonably well with the lowest energy band obtained from the simulations at the higher densities. The theory assumes that the cavity is perfectly spherical. Nonspherical fluctuations in the shape of the cavity lift the degeneracy of the excited state giving the different energy bands we observe in the simulation results.

In Fig. 8 we present x–y projections of the bound excess

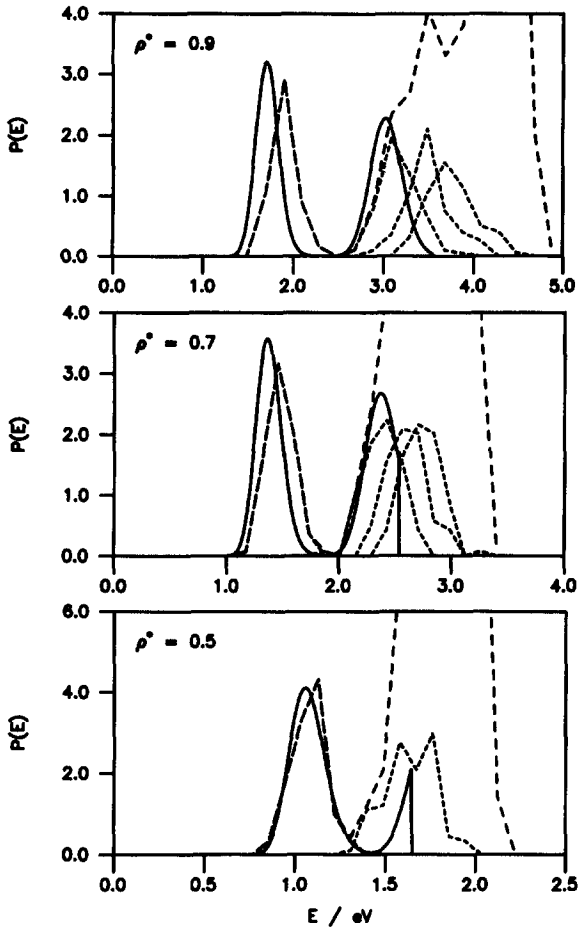

FIG. 7. Comparison of the excess electronic density of states predicted by the Wigner–Seitz model (solid curve) with that obtained from simulation (short dash curves indicate bound states and long dash curve is the total envelope). The first excited state band predicted by the Wigner–Seitz model is scaled down by a factor of 3.

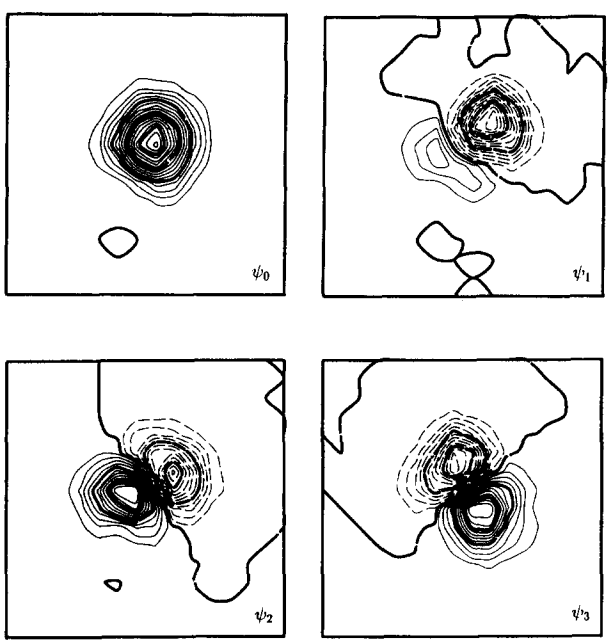

FIG. 8. Projections of the excess electronic wave functions onto the x–y plane for a configuration of fluid helium at the state point $T = 309$ K and $\rho^* = 0.9$. The lowest energy bound s- and p-like states are displayed. Dashed contours are negative values. The side length of the box is ~ 25.2 Å.

electronic wave functions obtained from our simulations for a typical configuration of the fluid atoms surrounding an excess electron in helium at $T = 309$ K and $\rho^* = 0.9$. The ground state electronic wave function is roughly spherical being s-like in character. The three excited states shown here are roughly cylindrical and they are each cut by a single, fairly complicated, nodal surface. These excited states are thus p-like in character. If the electron was moving in a perfectly spherical cavity then the three p-like states would be degenerate. Since in our simulations the cavity is randomly distorted from one solvent configuration to the next, this degeneracy is removed and we see three different energy states. As mentioned above, the Wigner–Seitz model assumes a perfectly spherical cavity so these p-like states are degenerate. Since the theory ignores nonspherical fluctuations it cannot predict the true inhomogenous linewidth. As we have already observed the theory can however give information about the contribution of spherical fluctuations to the linewidth from the scaled particle theory distribution of cavity sizes.

The bound state energies for an electron in a bubble of radius R_e predicted by the Wigner–Seitz model at various fluid densities are presented in Table I where we also display the average eigenvalues of the bound s and p-like states obtained from our computer simulations. We see that the energies predicted by the Wigner–Seitz model lie within a few percent of our simulation results.

We have calculated the excess electronic absorption line shape by accumulating a histogram of the excitation energies of the electron in which each entry is weighted by the square of the dipole matrix element $|\langle i;\mathbf{R}|\mathbf{r}|f;\mathbf{R}\rangle|^2$. This histogram was averaged over many different fluid configurations $\mathbf{R}$. The Wigner–Seitz model can also be used to calculate the line shape. Again, the distribution of bubble sizes will give us an inhomogeneous broadening. We have only considered transitions from the ground state to excited states in these spectrum calculations. This ground state dominance assumption is justified at the state points considered here as we have seen that the ground state is well separated from the excited states on the scale of thermal energies. This assumption will not be true at lower densities.

The comparison between the simulated and theoretical absorption line shapes is shown in Fig. 9. In general, as the density is decreased the solvent cavity becomes larger and

TABLE I. Comparison of average eigenvalues obtained from numerical simulation with the equilibrium energies predicted by the Wigner–Seitz bubble model.

eV	$\rho^* = 0.9$	$\rho^* = 0.7$	$\rho^* = 0.5$
	Simulation		
E_0	1.90	1.48	1.08
E_1	3.17	2.40	1.64
E_2	3.49	2.61	
E_3	3.76	2.74	
	Theory		
E_0	1.68	1.35	1.05
E_1	3.07	2.37	1.65

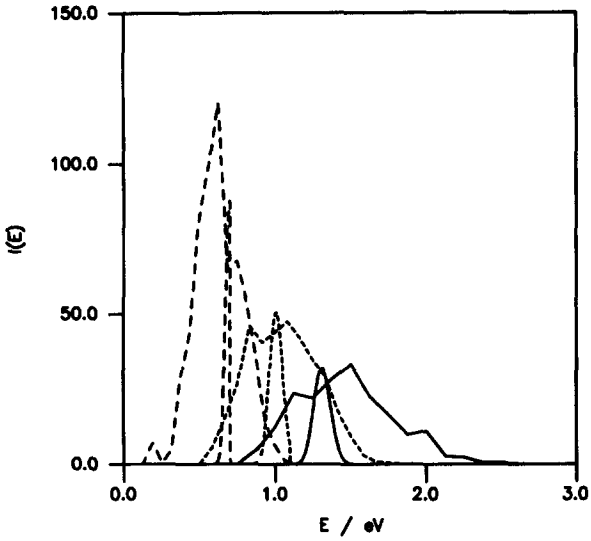

FIG. 9. Calculated absorption spectra for excess electrons in helium at $T = 309$ K for three densities: $\rho^* = 0.9$ (solid), $\rho^* = 0.7$ (short dash), and $\rho^* = 0.5$ (long dash). The broad bands are the simulation results while the narrow smooth curves are the predictions of the Wigner–Seitz model scaled down by a factor of 3. Absolute intensities in a.u.[2]

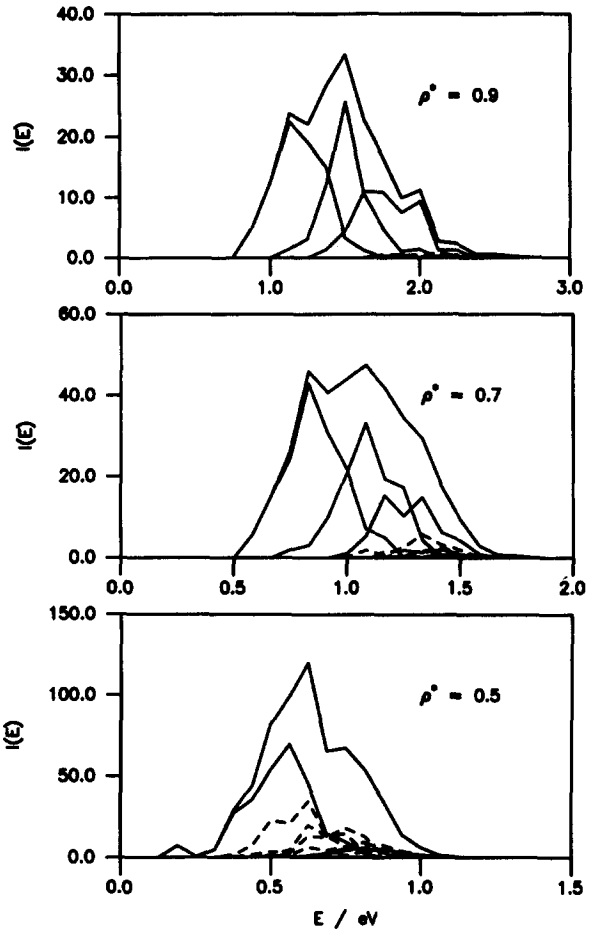

FIG. 10. Breakup of the spectra presented in Fig. 9 into the component bands associated with the various eigenvalues. Total envelope and bound state component bands are displayed as solid curves and the dash curves indicate continuum contributions. Absolute intensities in a.u.[2]

spacing between the electronic energy levels is smaller. This explains the red shift in the band center with decreasing density. The theory reproduces the density dependence of the band center quite accurately and also does reasonably well predicting the relative intensities at the different densities. As might be expected from our discussion of the density of states we see that the theoretical line shape is much narrower than that obtained from simulation due to the importance of nonspherical fluctuations in the cavity as discussed above.

In Fig. 10 we show how the broad electronic absorption line obtained from our simulation studies is in fact composed of several bands which result from transitions from the s-like ground state to various excited states. Transitions ending in continuum states are presented as dashed bands. At the lowest density we see that the continuum states are extremely important in determining the high energy tail of the absorption band.

The Thomas–Reiche–Kuhn sum rule states that for a Z electron system the oscillator strengths $f_{ks} = 2m_e/\hbar^2(E_k - E_s)|x_{ks}|^2$ for all the transitions originating from a given state $|s\rangle$ satisfy the following result:

$$\sum_k f_{ks} = Z,$$

where $x_{ks} = \langle k|x|s\rangle$. The sums of the oscillator strengths for the transitions between the ground state and the bound excited states in our one electron system at $\rho^* = 0.9$, 0.7, and 0.5 are, respectively, 0.86, 0.69, and 0.23. These results are averaged over the three Cartesian directions and over many configurations of the solvent. Thus bound to continuum state, transitions become important in the electronic absorption line shape as the solvent density is reduced. In fact if we sum the oscillator strengths over all the ten states included in our calculations at $\rho^* = 0.9$, 0.7, and 0.5 we find that the total oscillator strength associated with these states is 0.90, 0.81, and 0.61. Thus, at the lowest density the absorption line shape displayed in Figs. 9 and 10 is missing nearly 40% of the oscillator strength because the technique we use here only considers a small range of energy states in the continuum.

V. CONCLUSIONS

One result we have observed in this study is that the fluctuating potential wells experienced by an electron in a simple fluid become, on average, more shallow and able to support fewer bound states as the solvent density is decreased. At $\rho^* = 0.9$ in helium, e.g., we saw that the bubble could support the ground s-like state and three p-like excited states. At $\rho^* = 0.5$, on the other hand, only a single bound excited state was observed. For even lower solvent densities we expect that the ground state will also be enveloped by the continuum and that, on average, the density fluctuations in the fluid will be unable to support any bound excess electronic states. Under these circumstances the electron will have high mobility. This situation must arise in systems such as dense fluid xenon and other polarizable liquids where the electron mobility is observed to be very large at higher liquid densities.[21,22]

An interesting experiment which will give information about the validity of the Born–Oppenheimer–like approximation which we have made in these studies is to measure the excitation induced electronic mobility. When the electron is in a state which is bound to a density flucutation, the mobility will be determined by the motion of the entire bubble through the fluid. If we excite the electron to a higher energy bound state and the average cavity geometry does not change then the mobility should remain close to the value determined by the bubble motion in the ground electronic state. Deformation of the solvent cavity on electronic excitation and thus breakdown of our approximation would be signaled if the mobility was strongly dependent on the particular bound state into which we excite the electron. This experiment could be performed in helium at $\rho^* = 0.9$ since the three p-like states which are strongly dipole connected to the ground state are bound to the cavity. At $\rho^* = 0.5$, on the other hand, excitation could take the electron from a bound to a continuum state and high mobilities may be observed.

The Wigner–Seitz model makes some rather extreme approximations including treating the solvent as an ordered lattice of scatterers, thus ignoring the disorder and fluctuations in the fluid. Use of the averaged boundary condition at the edge of the bubble is analogous to turning the Born-Oppenheimer approximation upside down which should have rather serious dynamical consequences. However, despite all its inadequacies, we have demonstrated that this simple theoretical model gives a reasonable description of the bound states of an excess electron in fluid helium. A variety of properties calculated in our simulation studies compare quite well with the results predicted by the Wigner–Seitz model. The model is even able to predict the density dependence of the average electron bubble dissociation energy with reasonable accuracy.

Nichols and Chandler[23] have recently extended the equilibrium RISM-polaron theory, using analytic continuation techniques, to give excited state and dynamical information for electrons in simple fluids. The equilibrium version of this approximate theory gives results which agree quite well with computer simulation calculations[24] provided the hard sphere distance of closest approach d, describing the electron–solvent interaction, is adjusted appropriately.

The dynamical consequences of the approximations made in this theory have not yet been explored. In Fig. 11 we present a comparison between the absorption coefficient obtained from our simulations and that predicteed by the RISM-polaron theory. The theory treats the solvent as a hard sphere fluid, thus the density must be scaled appropriately, as disucssed earlier (i.e., $\rho^*_{HS} \sim 0.6\rho^*_{LJ}$), so that a comparison with the Lennard-Jones system can be made. We present the results of the RISM-polaron theory[25] with $\lambda = \hbar(\beta/m_e)^{1/2} = 6.62\sigma$ corresponding to the same temperature as our simulations and $d = 0.48\sigma$. Laria *et al.*[24] found that this value of d gave reasonable agreement between RISM-polaron theory and simulation for the equilibrium properties of an excess electron in fluid helium. From the figure we see that the agreement betweeen simulation and theory for this dynamical property is generally very satisfactory. The band position, absolute intensity, and low

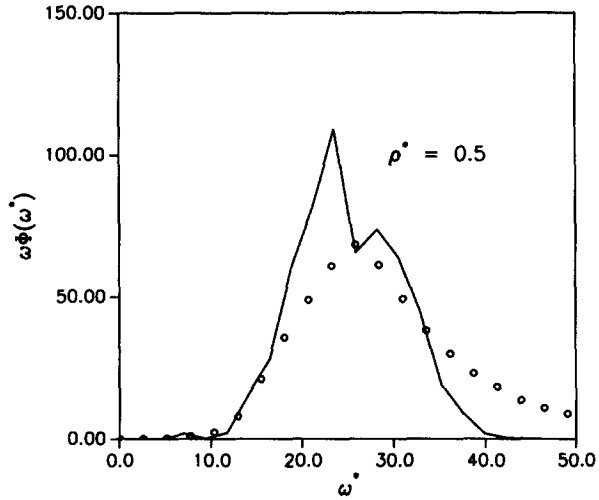

FIG. 11. Comparison of RISM-polaron theory absorption coefficient obtained with $d = 0.48\sigma$ (points) with our simulation results (curve). $\rho^*_{LJ} = 0.5$ and $T = 309$ K. Absolute intensities in a.u.^{2}, $\omega^* = \beta\hbar\omega$.

energy behavior are in good agreement. However, there is a discrepancy in the linewidth due to the appearance of a distinctive high energy tail in the RISM-polaron theory results which is not observed in our simulations.

This difference may result from the approximations made in the RISM-polaron theory. To obtain dynamical properties from the theory, Nichols and Chandler[23] analytically continue the so-called mean square displacement correlation function which depends on the spatial extent of the electronic distribution. Sprik, Klein, and Chandler[4] have compared path integral Monte Carlo calculations of this correlation function with RISM-polaron theory predictions for the hard sphere system. They find that the RISM-polaron theory overestimates the spatial extent of the electronic distribution in the regime of densities relevant to our comparison. By adjusting the hard sphere interaction diameter d to give agreement between the RISM-polaron theory predictions and equilibrium simulation results, Laria and Chandler have obained an effective potential which, when used in their approximate theory, gives a reasonable description of the average spatial extent of the electronic distribution. Once these geometrical considerations are well represented, the theory should give a good description of the band position. The line shape is determined by fluctations in the solvent and the electron distribution. In the RISM-polaron theory, fluctuations are represented using a mean field approximation . The accuracy of this approximation and the influence of adjustments in d on the fluctuations are not clear. Inadequate treatment of fluctuations may be the source of the difference in spectral line shape. The RISM-polaron theory involves several approximations and it would be useful to assess the accuracy of each one of these, where possible, using computer simulation.

Another explanation for this difference may be that our calculations give a poor representation of the high energy continuum states which may contribute to a tail. As noted earlier, and observed in Fig. 10, these states become very important at lower solvent densities. The experimental ex-

cess electronic absorption spectra in polar fluids such as water and ammonia all show a characteristic high energy tail. Simulation studies on these systems[6–8] have failed to reproduce this feature. By virtue of the use of periodic boundary conditions, these calculations all suffer from the same problem we have encountered when describing the continuum states and this inadequate treatment of the continuum states may be responsible for the failure to give the experimentally observed tail.

We would have liked to have made a more extensive test of the RISM-polaron theory. It is difficult to extend our calculations to much lower densities because of the inadequate treatment of the continuum states discussed above. We are developing new methods which should enable us to treat the continuum states more accurateley. Unfortunately, one encounters numerical problems when attempting to use the RISM-polaron theory to study systems at higher densities. The problems apparently result from the extreme differences in the various time scales of the electronic motion.[23] The electron moves very rapidly bouncing back and forth inside the bubble but the center of charge diffuses very slowly through the lattice of fixed scatterers. It is hoped that these problems with application of the RISM-polaron theory can be overcome so that a more complete test of the theory can be made by comparing its predictions with simulation over a wide range of densities.

It is important to note that all the theoretical and computational models discussed in this paper invoke the adiabatic approximation. When we did our path integral Monte Carlo calculations to obtain the various solvent configurations, the nuclei were moving over individual Born–Oppenheimer electronic energy surfaces with a Boltzmann probability distribution based on the electronic eigenvalues. The RISM-polaron theory calculations also make this approximation.[23] Nonadiabatic effects will become important when the energies of the different electronic states are close as they are for electrons in low density solvents.

In the polar fluids water[6,7] and ammonia[8] a detailed study of the onset of continuum state behavior with electronic excitation has not yet been conducted. However, the electronic wave functions in these polar fluids show well shaped contours localized around the region of the cavity even for states higher in energy than four to five excitations. Thus, the potential well which binds the electron to the cavity in these polar liquids must be considerably deeper than in helium. This is not really surprising as it has been observed that the polar molecules around the electron orient to form a clathrate cage on solvation. The electron attractive ends of the surrounding molecules arrange themselves to produce a deep negative potential region outside which the repulsive ends give rise to a high potential barrier. This structural organization of the fluid gives the very high bubble dissociation energies expected in these liquids.

The main extension of this work which we are currently pursuing is the development of both numerical and theoretical treatments of the continuum. From the energies listed for the states in Fig. 5 we see that the continuum states obtained from our simulations are in fact separated by a finite energy spacing on the order of the energy of the free particle state with wavelength equal to the periodic box dimension. This value gives the energy resolution of the technique. The reason we only explore a very small portion of the continuum band in our studies is because of the method we use to work our way sequentially up through the energy states. When we hit the continuum we spend all our time finding low lying states which are orthogonal to all those previously determined and there will be effectively an infinite number of such states. A more efficient approach which should give the major features of the band structure is to propagate a solution in real time which is held orthogonal to the bound states of the bubble and employ a spectral analysis of the real time correlation function similar to that described by Feit, Fleck, and Steiger.[9] We are currently developing this technique for performing band structure calculations in fluids. Similarly, we are extending the Wigner–Seitz model so that it might also handle continuum states.

ACKNOWLEDGMENTS

We wish to thank Peter Rossky for freely communicating his ideas on improving the efficiency of the split operator FFT algorithm before publication. We also would like to thank David Chandler for sending us his dynamical RISM-polaron theory results before publication. This work was supported by a grant from the NSF (NSF CHE-8201835 and CHE-8700522) and by a grant of supercomputer time from the NSF Office of Advanced Scientific Computing. The work was carried out at the NCSA, University of Illinois.

[1] B. E. Springett, M. H. Cohen, and J. Jortner, Phys. Rev. **159**, 183 (1967).
[2] A. L. Nichols III, D. Chandler, Y. Singh, and D. M. Richardson, J. Chem. Phys. **81**, 5109 (1984).
[3] D. Chandler, Y. Singh, and D. M. Richardson, J. Chem. Phys. **81**, 1975 (1984).
[4] M. Sprik, M. L. Klein, and D. Chandler, J. Chem. Phys. **83**, 3042 (1985).
[5] D. F. Coker, D. Thirumalai, and B. J. Berne, J. Chem. Phys. **86**, 5689 (1987).
[6] J. Schnitker, K. Motakabbir, P. J. Rossky, and R. A. Friesner, Phys. Rev. Lett. **60**, 456 (1988).
[7] A. Wallqvist, G. Martyna, and B. J. Berne, J. Phys. Chem. **92**, 1721 (1988).
[8] M. Sprik and M. L. Klein, J. Chem. Phys. **87**, 5987 (1987).
[9] M. D. Feit, Jr., J. A. Fleck, and A. Steiger, J. Comput. Phys. **47**, 412 (1982).
[10] P. J. Rossky (private communication).
[11] M. Vanhimbeeck, H. De Raedt, and D. Schoemaker, Phys. Rev. A **36**, 4612 (1987).
[12] R. C. Grimm and R. G. Storer, J. Comput. Phys. 134 (1971).
[13] J. B. Anderson, J. Chem. Phys. **63**, 1499 (1975).
[14] J. B. Anderson, J. Chem. Phys. **65**, 4121 (1976).
[15] D. M. Ceperley and B. J. Alder, Phys. Rev. Lett. **45**, 566 (1980).
[16] D. M. Ceperley and B. J. Alder, J. Chem. Phys. **81**, 5833 (1984).
[17] D. F. Coker and R. O. Watts, Mol. Phys. **58**, 1113 (1986).
[18] A. Selloni, P. Carnevali, R. Car, and M. Parrineollo, Phys. Rev. Lett. **59**, 823 (1987).
[19] H. Reiss, Adv. Chem. Phys. **9**, 1 (1965).
[20] L. Verlet, Phys. Rev. **165**, 201 (1965).
[21] M. A. Floriano and G. R. Freeman, J. Chem. Phys. **85**, 1603 (1986).
[22] J. A. Jahnke, L. Meyer, and S. A. Rice, Phys. Rev. A **3**, 734 (1971).
[23] A. L. Nichols III and D. Chandler, J. Chem. Phys. **87**, 6671 (1987).
[24] D. Laria and D. Chandler, J. Chem. Phys. **87**, 4088 (1987).
[25] D. Chandler (private communication).